scientific reports

Check for updates

OPEN

The response of meteorological drought to extreme climate in the water-receiving area of the Tao river diversion project in China

Huimin Hou[1], Di Lu[1]✉, Dongmeng Zhou[2], Junxing Bai[1], Feng Guo[1], Changjie Chen[1], Junde Wang[3], Yufei Cheng[4], Zhiqiang Bao[1] & Haohao Li[1]

Against the backdrop of increasing global extreme climate events, the water-receiving area of the Tao River Diversion Project in China frequently experiences drought disasters. In view of this, this study uses the meteorological drought index (SPEI) and 12 extreme climate indicators to analyze drought and extreme climate changes and their effects on drought. The results show that SPEI12 presents a slow but persistent downward trend, with 1988 as the turning point. Drought frequency exhibited a spatial pattern of being lower in the northwest and higher in the southeast. Additionally, droughts occurred more frequently but were of shorter duration. The summer days (SU) and warm days and warm nights (TX 90p, TN 90p) increased significantly. Although extreme precipitation events increased, the magnitude of change was not significant and thus could not effectively counteract the drought trend. Annual total precipitation (PRCPTOT), cold days (TX10p) and summer days (SU) are the main driving factors of meteorological drought, and their contribution rates are 23.35, 18.93 and 14.75% respectively. Annual total precipitation (PRCPTOT) and summer days (SU) have linear relationship with meteorological drought, and extreme climate indexes such as warm spell duration index (WSDI) and warm nights (TN90p) have nonlinear changes. Especially, the consecutive wet days (CWD) has a significant nonlinear change, when less than 8.58 days will lead to wetting, more than 8.58 days will lead to drought. In response to pressures from a warmer and drier future climate, the agricultural sector can build adaptive capacity. This can be achieved through the adjustment of planting structures, the promotion of water-saving technologies, and the incorporation of machine learning-derived thresholds into drought monitoring systems to enhance their early warning capabilities.

Against the backdrop of accelerating global climate change, the frequency and intensity of extreme climate events have increased markedly worldwide. Among these, droughts in particular have been occurring more often and with greater impact each year. As a widespread natural hazard exacerbated by global climate change, drought significantly threatens ecosystem stability and sustainable agricultural development[1]. China stands as one of the regions most vulnerable and sensitive to these changes[2], This is especially evident in the Loess Plateau and surrounding areas, where persistent drought has long constrained regional development. The Tao River Diversion Project, the largest inter-basin water transfer initiative in Gansu Province, has alleviated water scarcity issues in the receiving regions. However, against a background of rapid urbanization, increased rainfall variability, and more frequent extreme heat events, drought disasters are occurring more often and causing worsening economic losses. Traditional disaster management approaches are increasingly inadequate in addressing the compound challenges arising from the interplay of climate crises and human activities. Extreme climate events refer to those that fall in the tail of the statistical distribution of climate variables and have very low probabilities of occurrence. As a major category of such extremes, meteorological drought specifically describes a severe imbalance in the water budget caused by prolonged abnormal precipitation deficits coupled with anomalously high potential evapotranspiration.

[1]School of Civil and Hydraulic Engineering, Lanzhou University of Technology, Lanzhou 730000, China. [2]State Key Laboratory of Ecological Safety and Sustainable Development in Arid Lands Institute of Eco-Environment and Resources, Chinese Academy of Sciences, Lanzhou 730000, China. [3]Gansu Provincial Hydrology and Water Resources Center, Lanzhou 730000, China. [4]Gansu Academy for Water Conservancy, Lanzhou 730000, China. ✉email: 18119468680@163.com

Defined by a sustained imbalance where precipitation is insufficient to meet evapotranspiration demands, meteorological drought is a precursor to other forms of drought and plays a vital role in drought monitoring[3]. Numerous quantitative indices have been established in drought research, such as the Standardized Precipitation Index (SPI)[4], Standardized Precipitation Evapotranspiration Index (SPEI)[5], Standardized Runoff Index (SRI)[6], Self-Calibrated Palmer Drought Severity Index (scPDSI)[7] and a variety of other quantitative indicators. Different drought indicators represent different types of drought. These indices correspond to different drought categories; SPI and SPEI typically characterize meteorological drought, and SRI corresponds to hydrological drought. An ongoing controversy, however, surrounds whether SPEI and scPDSI should be classified as indicators of meteorological or agricultural drought. Comparative studies have indicated that on a global scale, scPDSI demonstrates a superior capacity over SPEI for characterizing agricultural drought[8].

In recent years, considerable progress has been made in understanding the relationship between drought dynamics and extreme climate events. However, most studies have focused primarily on the impacts of extreme climate on agricultural and hydrological droughts, while in-depth analysis of the nonlinear interactions between meteorological drought and extreme climate remains limited. For instance: Jehanzaib et al. applied the non-stationary GAMLSS algorithm to reveal how climate change and human activities influence hydrological drought across different time scales[9]; Shah et al. used multiple regression and ridge regression to analyze the effects of surface temperature and precipitation on wheat and rice yields[10]; B. et al. adopted the comprehensive ranking OME method to prioritize extreme climate indices affecting agriculture in the U.S. Corn Belt[11]; Jamalzi et al. assessed drought conditions in Afghanistan using the SPI and SPEI indices and performed correlation analyses with climatic variables such as maximum temperature (Tx) and minimum temperature (Tn) using Pearson correlation and linear regression[12]; YIN & BAI quantitatively evaluated the contributions of extreme climate variables to multi-scale meteorological drought across different climatic zones in the Yellow River Basin, China. Their results indicated that the Rx5day index is the dominant factor contributing to meteorological drought at various time scales, accounting for approximately 65% of the influence[13]; QU et al. employed wavelet spectrum analysis to quantify extreme climate conditions and their impact on hydrological drought in the Xilin River Basin of Inner Mongolia, China. They found a warming and drying trend in the region, where a significant increase in extreme temperature events, coupled with a lack of synchronous increase in extreme precipitation, has intensified hydrological drought risks[14]; Sifang et al. investigated changes in compound hydrological drought and extreme high temperature (CHDHE) events in China's semi-arid Luanhe River Basin from 1961 to 2016[15]. Although various methods are available to quantify the relationship between drought and extreme climate, their association is often not simply linear. Moreover, while existing research has largely centered on the effects of extreme climate or climate change on hydrological and agricultural droughts, further analysis is needed to elucidate the mechanisms through which extreme climate influences meteorological drought.

This study is designed to bridge this knowledge gap by pursuing three key objectives: first, to create a multidimensional portrait of the dynamics of extreme climate and meteorological drought by combining a suite of relevant indices; second, to decipher their interrelationships and lag effects using wavelet coherence and cross-wavelet analysis; and finally, to pinpoint the dominant drivers and unravel the nonlinear influence of extreme climate on drought through an integrated XGBoost-SHAP framework. Our goal is to clarify the underlying response mechanisms, providing actionable insights for this and other vulnerable regions worldwide.

Materials and methods

Overview of the study area

The Tao River is the second-largest tributary of the upper reaches of the Yellow River in China, with a total length of 673 km. The water-receiving area of the Tao River Diversion Project is located in the central part of Gansu Province, China, lying in the transition zone from the hilly and gully area of the Loess Plateau to the Longxi Loess Plateau, with an altitude ranging from 1137 to 3858 m. Dominated by landforms such as loess ridges, loess hills, and gullies, this region features diverse terrain with significant undulations. It suffers from severe soil erosion and high ecological environment sensitivity, making it one of the key areas for soil and water conservation on the Loess Plateau. In terms of topography, it presents a spatial pattern of being higher in the northwest and lower in the southeast. The overview map of the study area is shown in Fig. 1.

Data sources and processing

The Standardized Precipitation Evapotranspiration Index (SPEI) is sourced from the CHM_Drought dataset (https://zenodo.org/records/14634774). It is a raster dataset with a spatial resolution of $0.1° \times 0.1°$. This dataset is robust and capable of accurately capturing drought events across mainland China[16]. The extreme climate data are sourced from the National Cryosphere Desert Data Center of China (http://www.ncdc.ac.cn). It is an NC dataset with a spatial resolution of $0.1° \times 0.1°$. The annual drought and extreme climate data from 1985 to 2018 were selected, and subsequently, ArcMap 10.8 was used to perform clipping and masking processing on the downloaded data.

Extreme climate indices are based on the 27 extreme climate indices defined by the Expert Team on Climate Change Detection and Indices (ETCCDI). In this study, 12 of these commonly used extreme climate indices were selected for analysis[17] (Table 1).

Research methods

This study develops a comprehensive framework to analyze how meteorological drought responds to extreme climate conditions in the receiving area of China's Tao River Diversion Project. The framework comprises three integrated modules, as illustrated in Fig. 2: trend and mutation analysis, drought characterization, and driving factor analysis.

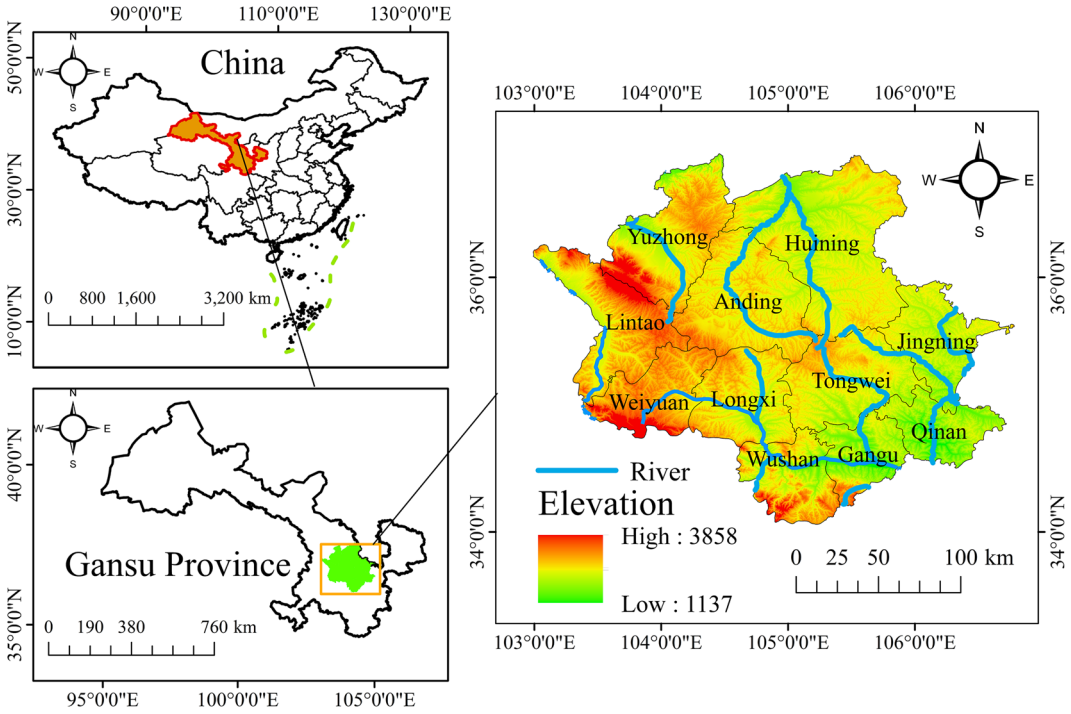

Fig. 1. Overview of the Study Area .Note: The figure made in ARCGIS10.8 (https://desktop.arcgis.com/zh-cn/index.html), the using of natural resources reproduction standard mapping (http://bzdt.ch.mnr.gov.cn/). The approval number is GS(2024) 0650, and the boundary of the base map is not modified.

Classifications	Acronyms	Title	Define	Unit
Extreme Temperature Index	SU	Summer Days	Number of days with daily maximum temperature TX > 25 °C	days
	TN10p	Cold Nights	Number of cold night days Percentage of days with daily minimum temperature < 10% quartile % of the year	%
	TX10p	Cold Days	Percentage of days with daily maximum temperatures < 10% quartile for the year	%
	TN90p	Warm Nights	Percentage of days with daily minimum temperature > 90% quartile for the year	%
	TX90p	Warm Days	Percentage of days with daily maximum temperature > 90% quartile for the year	%
	WSDI	Warm Spell Duration Index	Percentage of days with maximum temperature > 90% quartile for 6 consecutive days of the year days	days
	CSDI	Cold Spell Duration Index	Percentage of days with minimum temperature < 10% quartile for 6 consecutive days in a year days	days
Extreme precipitation index	SDII	Simple Daily Intensity Index	Ratio of total precipitation on wet days (daily precipitation ≥ 1.0 mm) to the number of wet days mm/day	mm/day
	R20mm	Days with Precipitation ≥ 20mm	Number of days with daily precipitation ≥ 20 mm in a year	days
	CWD	Consecutive Wet Days	Maximum number of consecutive days with precipitation ≥ 1 mm days	days
	R95pTOT	Total Precipitation on Very Wet Days	100*r95p / PRCPTOT	%
	PRCPTOT	Annual Total Precipitation	Sum of precipitation in a year	mm

Table 1. Definitions of extreme climate indicators.

(a) Trend and Mutation Point Analysis: Interannual trends (1985–2018) in meteorological drought and twelve extreme climate indices were evaluated using a combination of linear regression, Sen's slope test, and the Mann–Kendall test. The Innovative Trend Analysis (ITA) method provided graphical validation of these trends. Key mutation points in the time series were subsequently identified using the Sequential Mann–Kendall test.

(b) Drought Characterization and Cycle Identification: Based on run theory, key characteristics—average duration, severity, and intensity—of drought events were extracted from the SPEI12 series. The spatial frequency of different drought grades was also mapped. Wavelet coherence and cross-wavelet analyses were then applied to identify resonance periods, phase relationships, and lag effects between SPEI12 and extreme climate indices across multiple time scales.

(c) Driving Factor Analysis: A two-stage analytical approach was employed to identify key drivers. First, Pearson correlation analysis was used to prescreen extreme climate indices significantly associated with SPEI. Next, an optimized XGBoost model, tuned via Bayesian optimization, was constructed to predict SPEI12.

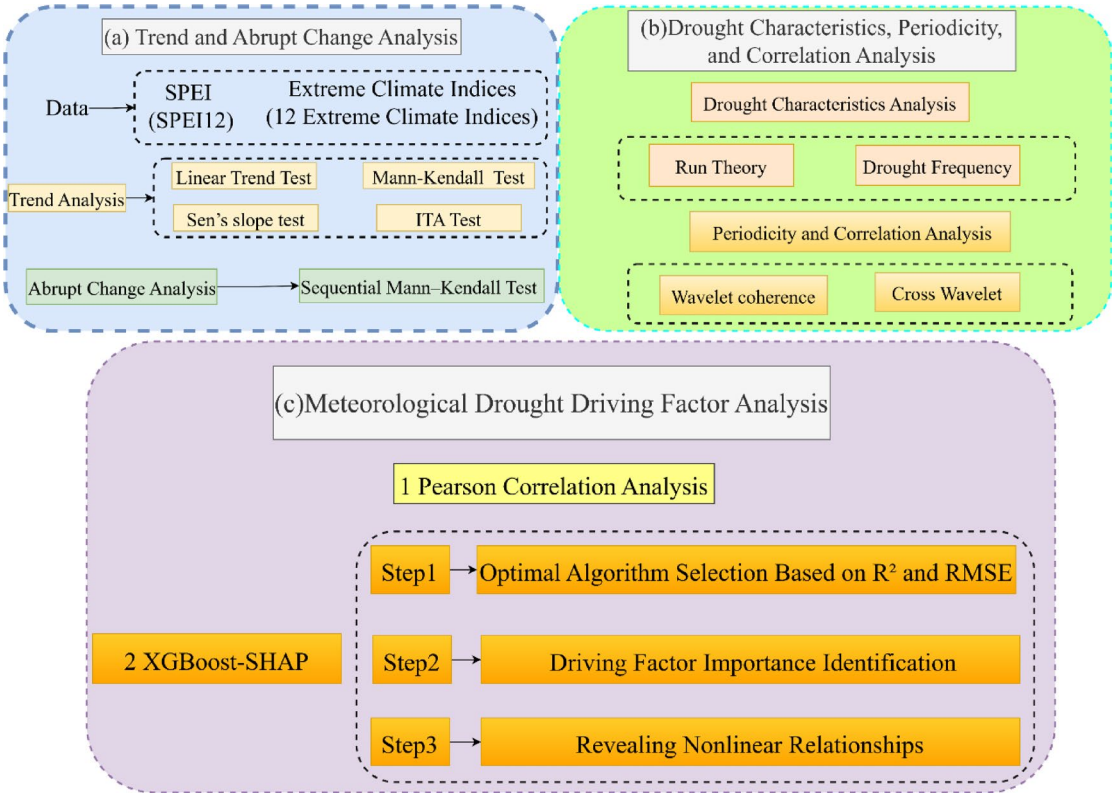

Fig. 2. Flow chart of research methods.

Drought level	Drought type	SPEI range
1	No Drought	SPEI > −0.5
2	Mild Drought	−1.0 < SPEI ≤ −0.5
3	Moderate Drought	−1.5 < SPEI ≤ −1.0
4	Severe Drought	−2.0 < SPEI ≤ −1.5
5	Extreme Drought	SPEI ≤ −2.0

Table 2. Evaluation grades of drought severity.

The SHAP framework quantified the contribution of each influencing factor, while dependence plots illustrated the nonlinear effects and critical thresholds of the principal drivers.

Standardized precipitation evapotranspiration index

The Standardized Precipitation Evapotranspiration Index (SPEI) is an indicator developed based on the Standardized Precipitation Index (SPI)[5], The Standardized Precipitation Evapotranspiration Index (SPEI) comprehensively considers meteorological factors such as temperature, precipitation, and evapotranspiration. It can stably assess the spatiotemporal characteristics of drought across multiple spatiotemporal scales and has been widely applied at present[18,19]. According to China's national standard GB/T 20,481–2017 Meteorological Drought Grades, the SPEI drought grades are divided into 5 levels (Table 2).

Trend and mutation analysis

The Mann–Kendall non-parametric test (abbreviated as M–K test)[20,21], Sen's slope test[22], and ITA (Interactive Trend Analysis) method were employed to analyze the interannual characteristic changes and trendality of the Standardized Precipitation Evapotranspiration Index (SPEI) and 12 extreme climate indices in the water-receiving area of the Tao River Diversion Project. Among these methods, the ITA test can provide complementary visualized result s of trends. To validate the Mann–Kendall (M–K) trend test, a linear trend test was used for cross-validation[23,24]. (see Table 3 for the results of spatial trend classification).

For the M–K trend test, at a given significance level α, if $|z| > z_{\alpha/2}$, it indicates that the hypothesis of no trend is rejected, and the time series data exhibit an obvious trend change. When |z| is greater than 1.645, 1.96 and 2.58, the trend is considered to have passed the significance test, with confidence levels of 90, 95 and 99%, respectively[25].

Classifications	Sen's slope test(β)	M–K Trend Test (Z)	Significance of trend change
1	β > 0	Z ≥ 2.58	Extremely Significant Increase
2	β > 0	2.58 > Z ≥ 1.96	Significant Increase
3	β > 0	1.96 > Z ≥ 1.645	Slight Increase
4	β > 0	Z < 1.645	Not-significant Increase
5	β < 0	Z ≥ 2.58	Extremely Significant Decrease
6	β < 0	2.58 > Z ≥ 1.96	Significant Decrease
7	β < 0	1.96 > Z ≥ 1.645	Slight Decrease
8	β < 0	Z < 1.645	Not-significant Decrease
9	β = 0		No Change

Table 3. Statistics of spatial trend changes.

The Interactive Trend Analysis (ITA) procedure begins by dividing a long-term time series into two consecutive sub-intervals of equal length, each sorted in ascending order. The data from the first sub-interval are plotted on the x-axis of a Cartesian coordinate system, and the data from the second on the y-axis. A diagonal line (45°) serves as a reference, bisecting the coordinate plane into upper and lower triangular areas. The trend of the time series is interpreted from the scatter plot as follows: data points distributed along the diagonal indicate stationarity (no trend); points accumulating in the upper triangle denote an increasing trend; and points in the lower triangle signify a decreasing trend. Non-monotonic trends can be precisely characterized by categorizing the data into low, medium, and high-value groups for separate analysis. Comprehensive computational details are available in[26].

Currently, there are several methods for identifying mutation points, including the M–K test[27], Pettit test[28,29], and heuristic segmentation method[30]. However, uncertainties may exist in the identification of mutation points for drought and extreme climate. Compared with the traditional M–K test, the Sequential Mann–Kendall test is more suitable for mutation analysis, and its core advantage lies in its ability to identify multiple mutation points in a time series. The Sequential Mann–Kendall test is a sequential version of the Mann–Kendall test[31,32] and enables more distinct identification of mutation points based on the significance value (α). Specifically, it first locates points where variables shift abruptly, then finds the intersection of the forward and backward sequences with the highest significance values. If this value falls within the confidence interval, the mutation point is determined based on the breakpoints with high significance values[33].

Run theory

Run theory is a time series analysis method that has been widely used to extract drought characteristics[34,35]. In this study, drought identification was conducted based on the annual-scale Standardized Precipitation Evapotranspiration Index (SPEI). According to the drought grade classification, a drought event occurs only when SPEI ≤ -0.5, with a minimum drought duration of 1 year. The number of drought events, average duration (D), severity (S), and intensity (L) of droughts in the water-receiving area of China's Tao River Diversion Project were calculated. The average values can comprehensively reflect the long-term drought characteristics of the region, and the specific calculation formulas are as follows:

$$D = T_{end} - T_{start} + 1 \tag{1}$$

$$S = \sum_{t=T_{start}}^{T_{end}} |SPEI| \tag{2}$$

$$L = \frac{S}{D} \tag{3}$$

Drought occurrence frequency

The drought occurrence frequency (P) refers to the degree of drought occurrence within a specific time period.

$$P = \frac{n}{N} \times 100\% \tag{4}$$

where: n is the number of years with a specific grade of drought, and N is the total number of years in the study period. In this study, the total frequency of mild, moderate, severe, extreme droughts, as well as the overall drought frequency, were analyzed respectively based on the pixel-wise SPEI12.

Wavelet coherence and cross-wavelet

Wavelet Coherence (WTC) describes the consistency of changes between two sequences across different time scales[36,37]. To enhance the analytical ability in high-energy regions, the Cross Wavelet Transform (XWT) is simultaneously used to analyze the correlation characteristics between the Standardized Precipitation Evapotranspiration Index (SPEI) and extreme climate indices in high-energy regions.

In this analysis, colors denote the relative energy density, while the thin black solid line defines the cone of influence (COI), within which the spectral values are considered valid. The black contours inside the COI delineate regions exceeding the 95% confidence level ($\alpha = 0.05$). The phase relationship between the SPEI and extreme climate indices is indicated by the arrow direction: rightward for a positive phase and leftward for a negative phase. Concurrently, the arrow orientation reveals the lead-lag dynamics: an upward orientation denotes that the SPEI lags the extreme index, and a downward orientation denotes that the SPEI leads it.

Driving factor analysis based on XGBoost and SHAP

Pearson correlation analysis was used to examine the relationship between meteorological drought and extreme climate indices. To further clarify the response of meteorological drought to extreme climates, machine learning (among 6 machine learning models, XGBoost performed the best) combined with SHAP analysis was adopted to determine the contribution degree of different extreme climate indices to meteorological drought. The XGBoost algorithm is an efficient ensemble learning method, commonly used for predicting high-dimensional data. By gradually optimizing the objective function and constructing weighted decision trees, it can capture nonlinear relationships[38].The Shapley Value method can be used to evaluate the contribution of various extreme climates to the prediction results of meteorological drought. By calculating the marginal contribution of features, SHAP (SHapley Additive exPlanations) can reveal the impact of each factor on meteorological drought[39]. The XGBoost-SHAP method provides deeper insights into climate driving mechanisms and uncovers complex interdependencies that may be overlooked by traditional analyses[10].

Results and analysis

Spatiotemporal variation analysis of meteorological drought

This study analyzed the 12-month Standardized Precipitation Evapotranspiration Index (SPEI12) in the water-receiving area of the Tao River Diversion Project from 1985 to 2018. As shown in Fig. 3a, the region experienced considerable fluctuations in meteorological drought, with the SPEI12 exhibiting a non-significant downward trend at a rate of -0.04 per decade ($Z_{m\text{-}k} = -0.55$, $\beta_{sen's} = -0.006$). A distinct wet-to-dry transition was also observed between 1992 and 1997.

To complement these findings, trend variations across different value ranges were visualized using the Interactive Trend Analysis (ITA) test (Fig. 3b). The results indicated relatively stable SPEI12 values in the high-value zone, a decrease at 62% of the points in the medium-value zone, and non-significant fluctuations in the low-value zone. These outcomes were consistent across the linear trend, Mann–Kendall (M–K), Sen's slope, and ITA tests.

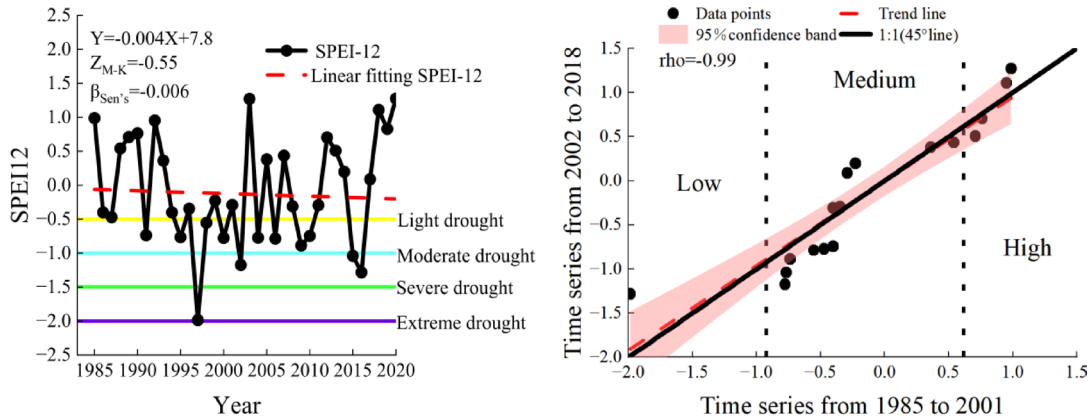

(a) SPEI trend Test from 1985 to 2018 (b) ITA SPEI trend changes

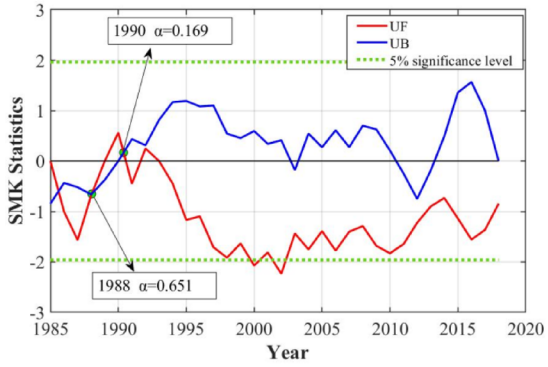

(c) M-K Mutation Point Test

Fig. 3. Analysis of Meteorological Drought Trend Mutation from 1985 to 2018.

The Sequential Mann–Kendall test was further applied to identify abrupt drought shifts. Figure 3c reveals statistically significant mutation points in 1988 and 1990, with the highest significance ($\alpha = 0.651$) occurring in 1988. Thus, a meteorological drought mutation was confirmed in 1988. Additionally, the UF statistic remained below zero after 1992, indicating a progressive intensification of aridity in the study area from that year onward.

Based on the Sen's slope estimator and Mann–Kendall (M–K) trend test, this study examined the spatial variation characteristics of meteorological drought in the water-receiving area of China's Tao River from 1985 to 2018 (Fig. 4).

As illustrated in Fig. 4a, the region overall exhibited a persistent drying trend during the study period. Specifically, the northwest showed a slight or non-significant decrease in SPEI values, indicating a tendency toward aridification over the long term. In contrast, most of the southeast experienced a non-significant increase in SPEI, suggesting a gradual shift toward humidification.

Analysis of the spatial distribution of the mean annual SPEI (Fig. 4b) further revealed relatively high values (indicating wetter conditions) in the northwest and parts of the east—likely influenced by monsoon patterns—while the southern and central parts showed relatively low SPEI values, reflecting drier conditions.

Spatial distribution of drought event characteristics

Based on the run theory, this study conducted a pixel-wise drought analysis using SPEI12 data, with drought events defined as periods where SPEI ≤ –0.5 lasting at least one year.

The results (Fig. 5) reveal that the highest frequency of drought events occurs in the southeastern part of the water-receiving area of the Tao River Diversion Project, with up to 11 recorded episodes. In contrast, the western areas experienced the fewest droughts, with only 6 events, while the central and northern regions showed moderate occurrence. In terms of average duration, droughts tended to persist longer—up to 3 years—in the southeast and parts of the central region, whereas shorter durations were observed elsewhere. A similar spatial pattern was found for average severity, with higher values (up to 3.14) in the southern and western regions and lower values in the remaining areas.

Notably, the spatial distribution of average drought intensity exhibited an inverse pattern to that of duration: high values were concentrated in the northwest and low values in the southeast. Overall, although the southern region experienced fewer drought events, those that did occur were relatively prolonged. Conversely, in the drought-prone east, the duration of individual events was generally shorter.

Figure 6 displays the spatial distribution of drought frequency at the annual scale. Mild droughts occur primarily in the southeastern and central parts of the region, while their frequency is notably lower in the northwest. In contrast, the pattern for moderate drought is essentially the inverse, with a higher frequency in the northwest and a lower frequency in the southeast. Severe drought occurrences are relatively uniform across the entire study area. Extreme droughts, however, are concentrated mainly in the central and western zones and are absent elsewhere. In summary, while the southeastern region experiences more frequent droughts overall, the northwestern area has a higher propensity for moderate drought.

Spatiotemporal variation analysis of extreme climate indices

Analysis of extreme climate indices in the water-receiving area of the Tao River Diversion Project reveals distinct warming trends and subtle shifts in precipitation patterns (Fig. 7 and Table 4). For temperature-related indices, a marked increase was observed in summer days (SU) at a rate of 4.4 d/10a, suggesting more frequent

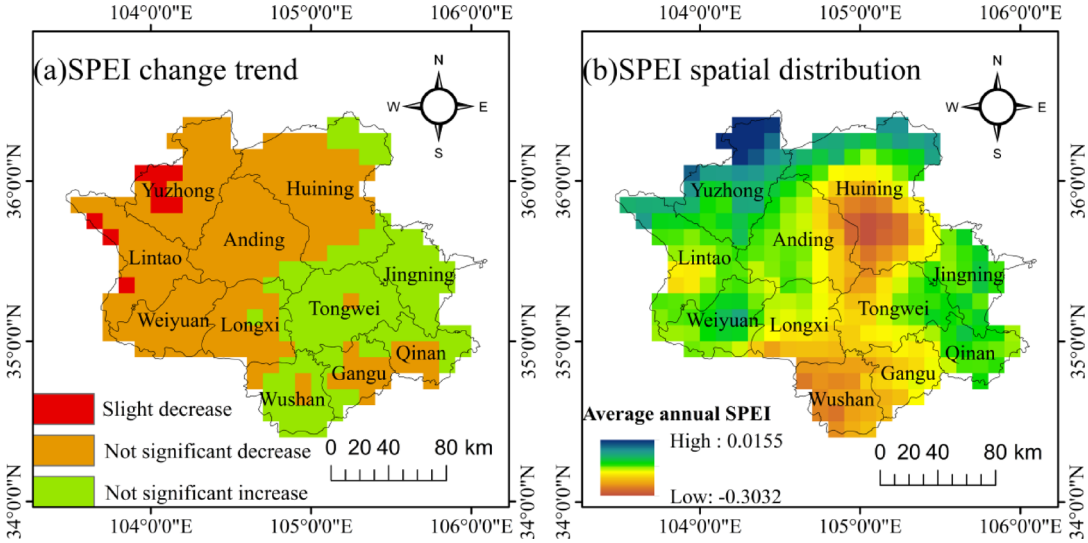

Fig. 4. Spatial Variation Trend and Distribution of Meteorological Drought. Note: The figure made in ARCGIS10.8 (https://desktop.arcgis.com/zh-cn/index.html), the using of natural resources reproduction standard mapping (http://bzdt.ch.mnr.gov.cn/). The approval number is GS(2024) 0650, and the boundary of the base map is not modified.

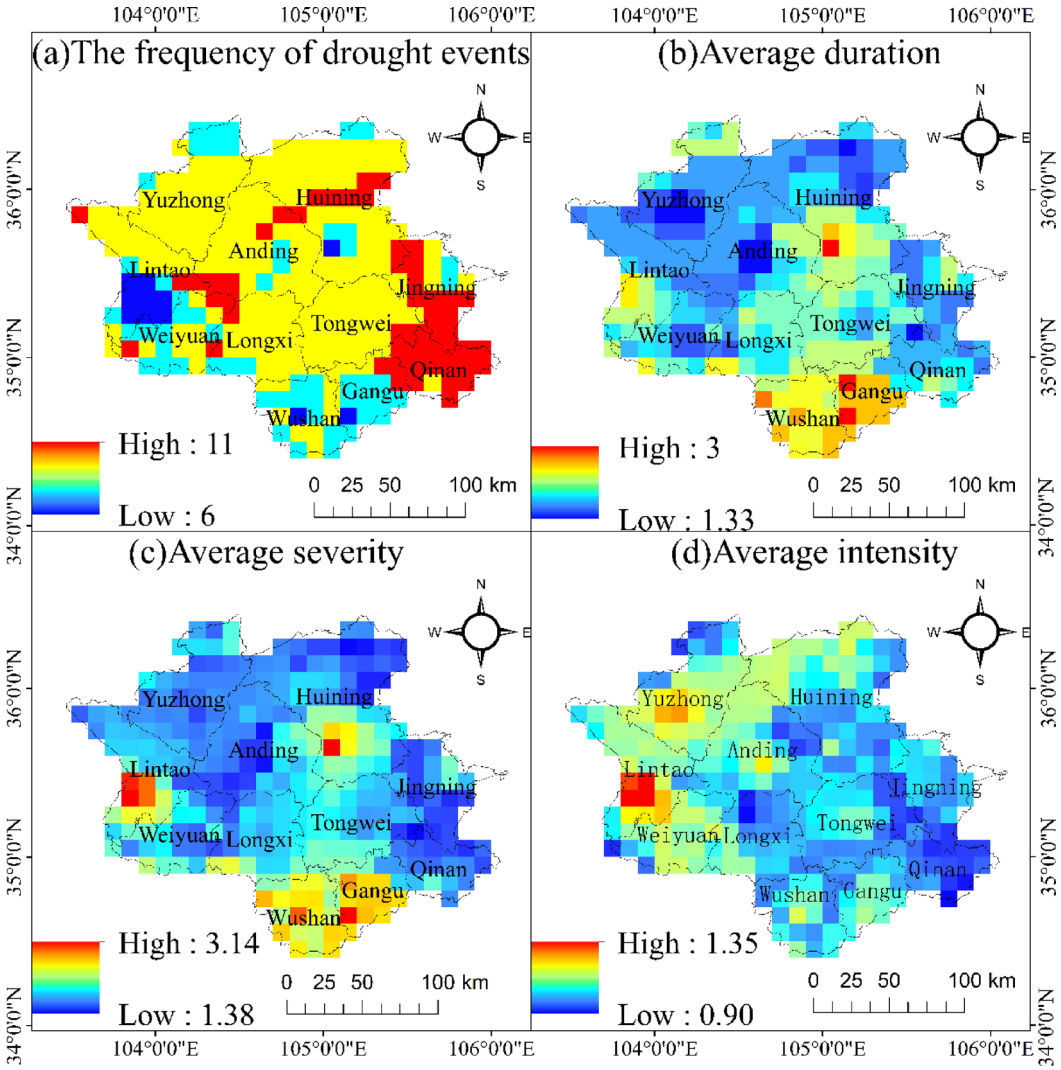

Fig. 5. Distribution of Drought Event Characteristics. Note: The figure made in ARCGIS10.8 (https://desktop.arcgis.com/zh-cn/index.html), the using of natural resources reproduction standard mapping (http://bzdt.ch.mnr.gov.cn/). The approval number is GS(2024) 0650, and the boundary of the base map is not modified.

intense warm events. Concurrently, cold nights (TN10p) decreased significantly (− 1.5%/10a), while cold days (TX10p) declined insignificantly (− 1.2%/10a). In contrast, both warm nights (TN90p) and warm days (TX90p) increased significantly, by 3.9%/10a and 2.3%/10a, respectively. The warm spell duration index (WSDI) also rose significantly (1 d/10a), whereas the cold spell duration index (CSDI) showed an insignificant decrease (− 0.2 d/10a). Collectively, these results indicate that the magnitude of increase in extreme warm indices substantially exceeds the decrease in extreme cold indices.

Among precipitation indices, only the Simple Daily Intensity Index (SDII) increased significantly, by 0.2 (mm/day)/10a. Other indices, including theDays with Precipitation ≥ 20mm (R20mm; 0.4 d/10a), total precipitation on very wet day (R95pTOT; 2.2%/10a), and the annual total precipitation (PRCPTOT; 23.9 mm/10a), exhibited insignificant upward trends. Consecutive wet days (CWD) decreased insignificantly (− 0.3 d/10a). Although most precipitation trends are not statistically significant, they collectively suggest a potential tendency toward future humidification in the region.

The variation trends identified were consistent across the linear trend, Mann–Kendall, and Sen's slope tests.

Between 1985 and 2018, the water-receiving area of the Tao River Diversion Project exhibited considerable spatial heterogeneity in extreme climate indices (Fig. 8).

The summer days (SU) ranged from 6.65 to 88.74 days—a 13.4-fold difference—with higher values in the periphery and lower values in the central area. The spatial distributions of cold nights (TN10p) and cold days (TX10p) were similar, with higher frequencies in the northwest and central parts and lower frequencies in the southeast. Their maximum values reached 10.22% and 10.24%, and minimum values were 8.78% and 9.38%, respectively.

In contrast, warm nights (TN90p) and warm days (TX90p) both reached their maxima in the southeast, with minima located in the northwest and central regions, respectively. The spatial pattern of the warm spell

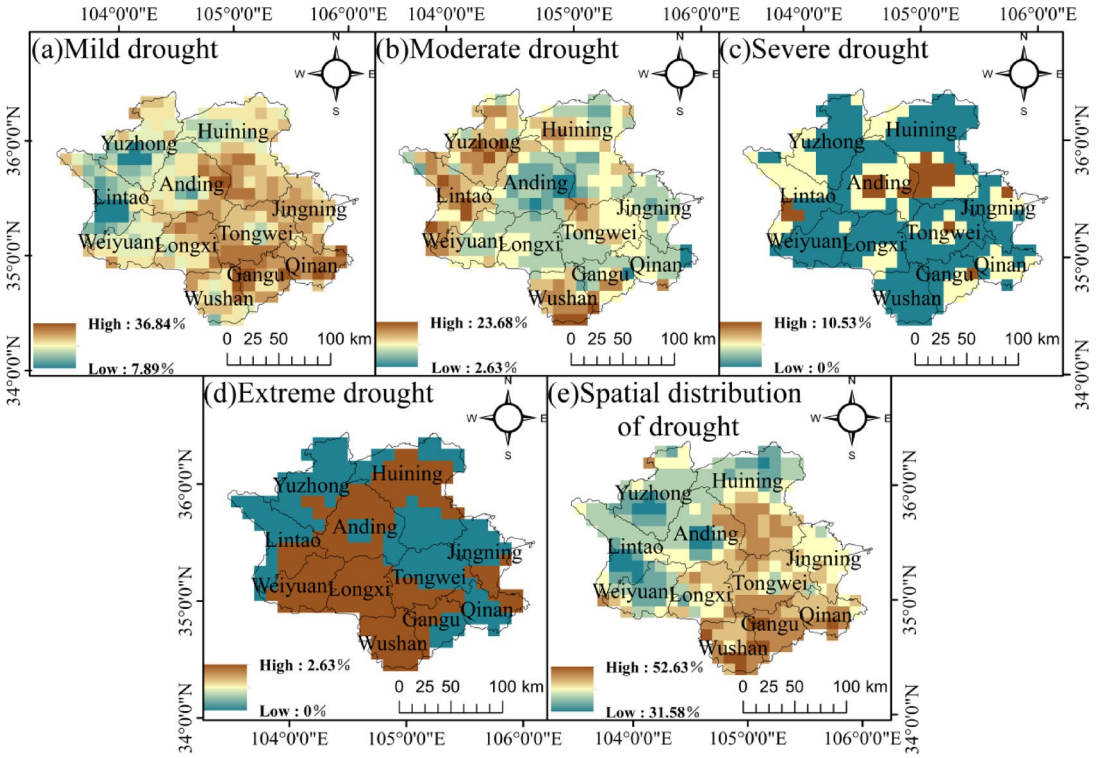

Fig. 6. Spatial Distribution of Drought Frequency. Note: The figure made in ARCGIS10.8 (https://desktop.arcgis.com/zh-cn/index.html), the using of natural resources reproduction standard mapping (http://bzdt.ch.mnr.gov.cn/). The approval number is GS(2024) 0650, and the boundary of the base map is not modified.

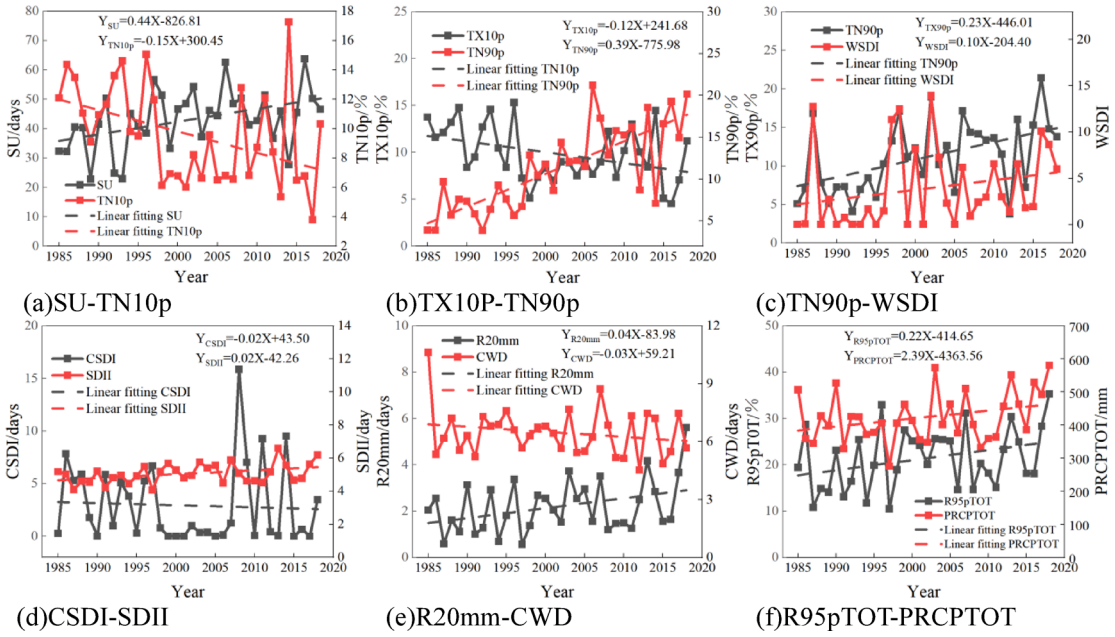

Fig. 7. Linear trend test of extreme climate.

duration index (WSDI) resembled that of warm days. The cold spell duration index (CSDI) showed marked spatial variation, with a maximum value of 7.59 days concentrated in the south, while most other areas recorded a minimum of 1 day.

Among precipitation-related indices, the simple daily intensity index (SDII) and Days with Precipitation ≥ 20mm(R20mm) shared a similar spatial structure—low in the north and south, high in the east and west. Both

Norm	CODING	M–K trend test			Sen's slope test
		Z_{M-K}	movement	Significance	β
Summer Days	SU	2.3719	Up	*	0.4116
Cold Nights	TN10p	− 2.7277	Low	**	− 0.1716
Cold days	TX10p	− 1.8975	Low		− 0.1176
Warm Nights	TN90p	5.0107	Up	**	0.4329
Warm Days	TX90p	3.0835	Up	**	0.2762
Warm Spell Duration Index	WSDI	2.2830	Up	*	0.1046
Cold Spell Duration Index	CSDI	− 1.0377	Low		− 0.0174
Simple Daily Intensity Index	SDII	2.0754	Up	*	0.0228
Days with Precipitation ≥ 20mm	R20mm	1.8382	Up		0.0345
Consecutive Wet Days	CWD	− 0.7857	Low		− 0.0163
Total Precipitation on Very Wet Days	R95pTOT	1.6603	Up		0.2058
Annual total precipitation	PRCPTOT	1.5121	Up		2.2174

Table 4. Statistical table of extreme climate trend tests. **is the significance level of α = 0.01;* is the significance level of α = 0.05.

consecutive wet days (CWD) and annual total precipitation (PRCPTOT) decreased from south to north. In contrast, the total precipitation on very wet days (R95pTOT) was lower in the central area and higher in the surrounding regions.

For extreme climate indices with multiple mutation points identified, the most statistically significant point from the Sequential Mann–Kendall test was selected as the definitive mutation year. As summarized in Table 5, a significant mutation in meteorological drought occurred in 1988.

The mutation points for extreme temperature indices—including warm nights (TN90p), warm days (TX90p), summer days(SU), cold nights(TN10p), cold days(TX10p)—were concentrated between 1990 and 2000, showing a slight lag relative to the 1988 drought mutation. Similarly, mutation points for extreme precipitation indices (SDII, R20mm, R95pTOT) generally occurred later, with most emerging after 2000. Specifically, the simple daily intensity index (SDII) and the total precipitation on very wet days (R95pTOT) mutated between 2007 and 2008, whereas the days with precipitation ≥ 20mm (R20mm) and annual total precipitation (PRCPTOT) shifted as late as 2015–2016.

This sequential pattern suggests that the mutation in meteorological drought is an integrated response to the combined effects of temperature and moisture, reacting more directly to global warming. In contrast, extreme precipitation depends not only on sufficient water vapor but also on specific atmospheric circulation patterns, making its triggering mechanisms more complex. This added complexity likely accounts for the observed lag in its mutation points.

Wavelet analysis of meteorological drought and extreme climate

A correlation analysis was conducted between the annual Standardized Precipitation Evapotranspiration Index (SPEI) and several extreme climate indices (Fig. 9), with the key findings summarized as follows.

Significant periodic resonances and phase relationships were identified between SPEI and specific extreme indices. For summer days (SU), cross wavelet transform (XWT) revealed a significant 3–4 year resonance period with a negative phase during 1990–1996, while wavelet coherence (WTC) showed strong correlations around the 4-year scale from 1990 to 2001 and a 4–5 year period during 2009–2012, both indicating SPEI lagging behind SU under a negative correlation. In the case of cold nights (TN10p), although XWT showed no significant resonance, WTC identified a relatively significant 0–3 year period with SPEI leading TN10p under weak negative correlation. For cold days (TX10p), WTC indicated high-energy resonances at 2–4 years (1990–1998) and 5–7 years (2008–2011), showing a positive correlation with SPEI leading. Regarding warm nights (TN90p), WTC detected significant resonances at 0–2 years (1990–1995) and 4–5 years (2009–2012), with upward-left arrows suggesting negative correlation and SPEI lagging. Finally, for warm days (TX90p), XWT indicated a sub-annual resonance during 2003–2006, while WTC revealed a significant 8–9 year period from 1996 to 2007, also reflecting negative correlation and SPEI lagging behind TX90p.Wavelet analysis of SPEI and the warm spell duration index (WSDI) revealed a significant 0–1 year resonance period during 1998–2001 in the XWT results. The WTC analysis further identified three significant resonance periods: two 0–1 year bands during 1987–1991 and 1997–1999, and an 8–10 year period during 1998–2007. All of these resonance periods exhibited a significant negative correlation, with SPEI lagging behind WSDI. For the cold spell duration index (CSDI), the XWT analysis showed no significant resonance period, although intermittent energy concentration was observed at the 0–7 year scale. In contrast, the WTC analysis detected a significant 0–1 year resonance period during 2001–2003, which also showed a significant negative correlation with SPEI lagging behind CSDI.

For precipitation-related indices, SPEI and both the simple daily intensity index (SDII) and the Days with Precipitation ≥ 20mm (R20mm) exhibited similar correlation patterns. The XWT results showed significant approximately 3-year resonance periods during 1993–1997 for SPEI-SDII and during 1992–1996 for SPEI-R20mm. The WTC analysis identified three common significant resonance periods: 0–8 years during 1998–2013, 0–7 years during 1998–2003, and 5–10 years during 1996–2015. All showed significant positive correlations

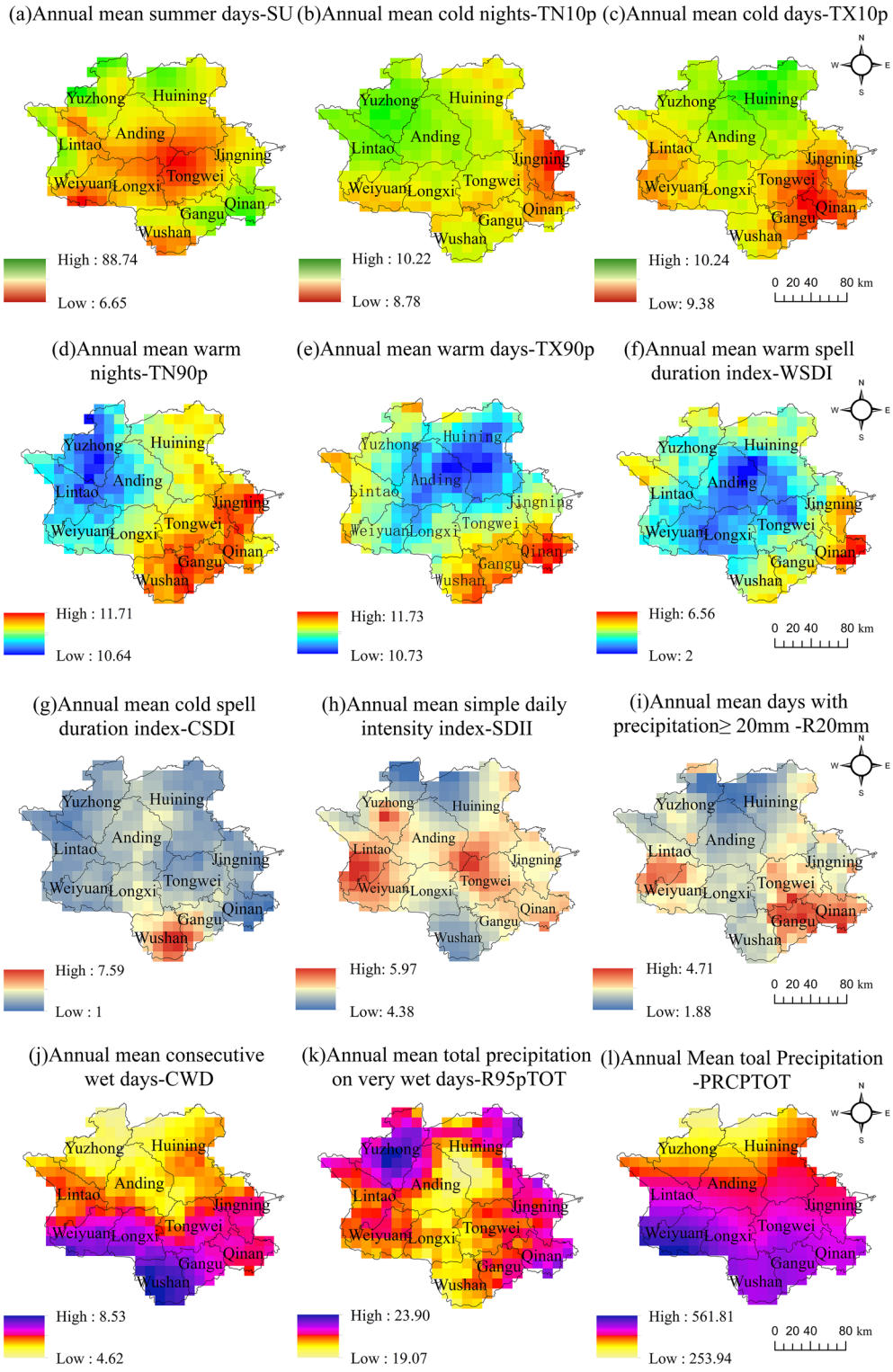

Fig. 8. Spatial Distribution of Extreme Climate Indices. Note: The figure made in ARCGIS10.8 (https://desktop.arcgis.com/zh-cn/index.html), the using of natural resources reproduction standard mapping (http://bzdt.ch.mnr.gov.cn/). The approval number is GS(2024) 0650, and the boundary of the base map is not modified.

with SPEI leading both SDII and R20mm. For consecutive wet days (CWD), the XWT revealed a significant approximately 6-year resonance period during 2007–2011, while the WTC analysis showed significant 0–1 year resonance periods during 1989–1990 and 2001–2003, as well as a significant 3–6 year period during 1990–2012. These correlations were significantly positive with SPEI lagging behind CWD. Regarding the total precipitation on very wet days (R95PTOT), the XWT detected a significant 2–3 year resonance period during 1992–1997,

Norm	Coding	Sequential Mann–Kendall test
Summer Days	SU	1991
Cold Nights	TN10p	1994
Cold Days	TX10p	1990
Warm Nights	TN90p	1999
Warm Days	TX90p	1996
Warm Spell Duration Index	WSDI	2010
Cold Spell Duration Index	CSDI	1989
Simple Daily Intensity Index	SDII	2008
Days with Precipitation ≥ 20mm	R20mm	2016
Consecutive Wet Days	CWD	1991
Total Precipitation on Very Wet Days	R95pTOT	2007
Annual total precipitation	PRCPTOT	2015

Table 5. Mutation point test of extreme climate indices.

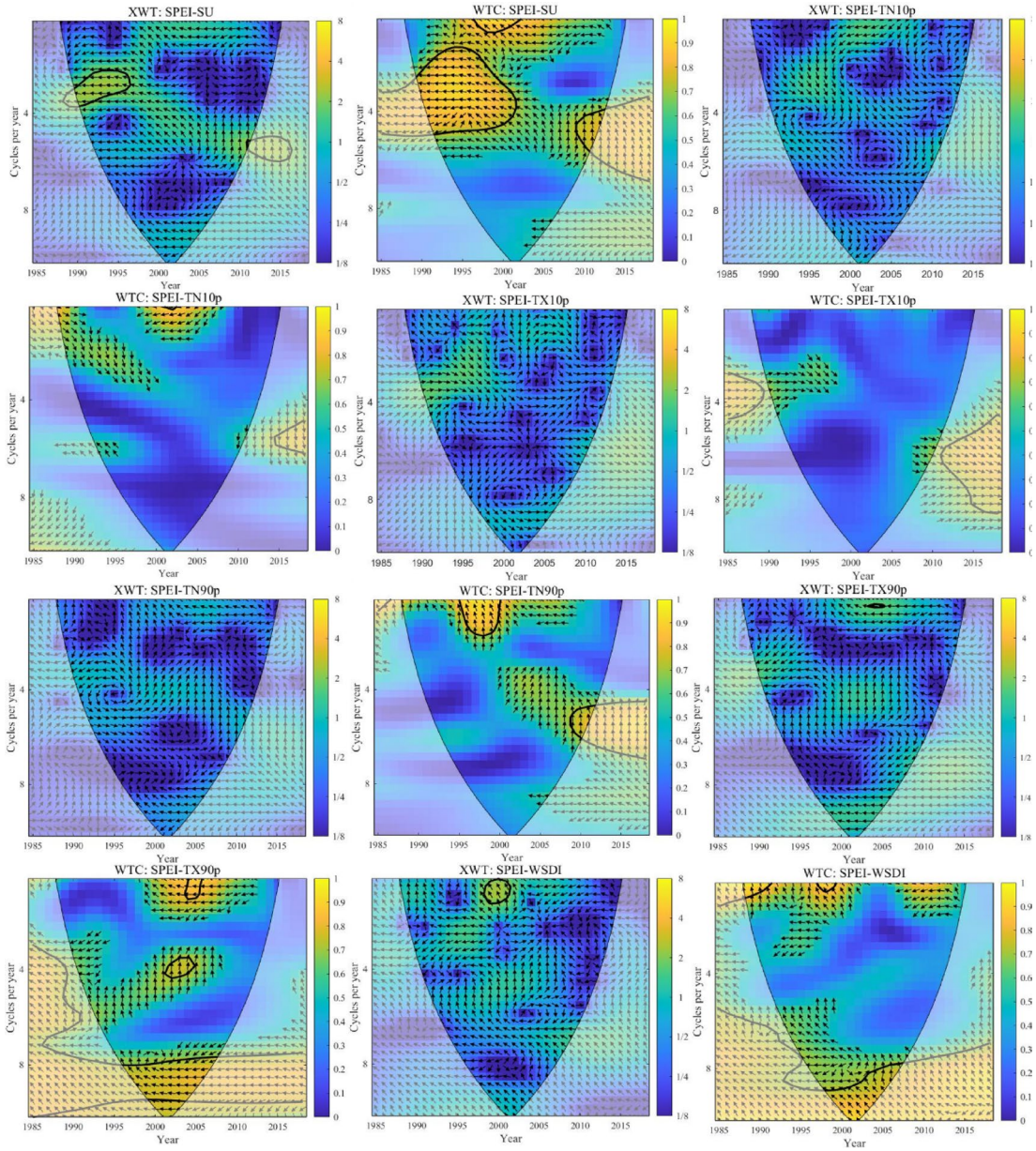

Fig. 9. Wavelet spectra of meteorological drought and extreme climate.

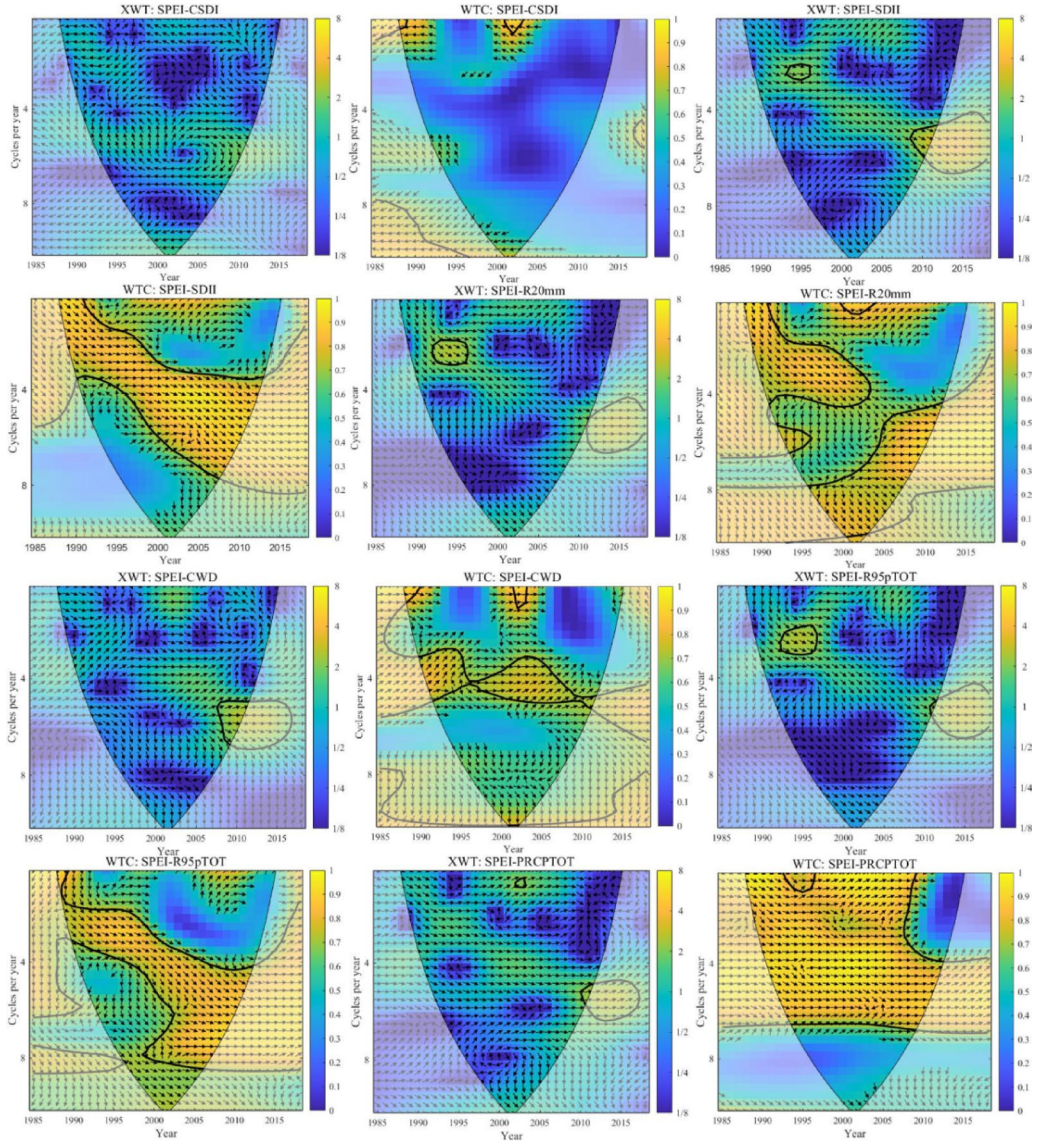

Fig. 9. (continued)

and the WTC analysis identified a significant 0–8 year period during 1998–2012, showing a significant positive correlation with SPEI leading. For annual total precipitation (PRCPTOT), the XWT indicated a significant less-than-1-year resonance period during 2002–2003, and the WTC analysis revealed a significant 0–6 year period during 1998–2012, exhibiting a significant positive correlation with SPEI leading.

Overall, the Standardized Precipitation Evapotranspiration Index (SPEI) exhibits a negative correlation with extreme temperature indices and a positive correlation with extreme precipitation indices. Specifically, SPEI lags behind several temperature-related indices— summer days (SU), warm nights (TN90p), warm days (TX90p), and warm spell duration index (WSDI)—while it leads several precipitation-related indices: cold nights (TN10p), cold days (TX10p), simple daily intensity index (SDII), days with precipitation ≥ 20mm (R20mm), total precipitation on very wet days (R95PTOT), and annual total Precipitation (PRCPTOT).

In terms of temporal dynamics, SPEI and many extreme temperature indices show significant resonance on short-time scales (under 5 years), reflecting the rapid influence of changing climatic conditions on drought. In contrast, certain extreme precipitation indices—SDII, R20mm, and consecutive wet days (CWD)—display significant resonance with SPEI on medium- to long-time scales (over 5 years), highlighting the long-term regulatory role of precipitation patterns in drought evolution.

Analysis of drought driving factors

Analysis of driving factors based on Pearson correlation

Pearson correlation analysis (Fig. 10) indicates that from 1985 to 2018, meteorological drought, as represented by the Standardized Precipitation Evapotranspiration Index (SPEI), exhibited distinct relationships with various extreme climate indices. SPEI was positively correlated with annual total precipitation (PRCPTOT), days with

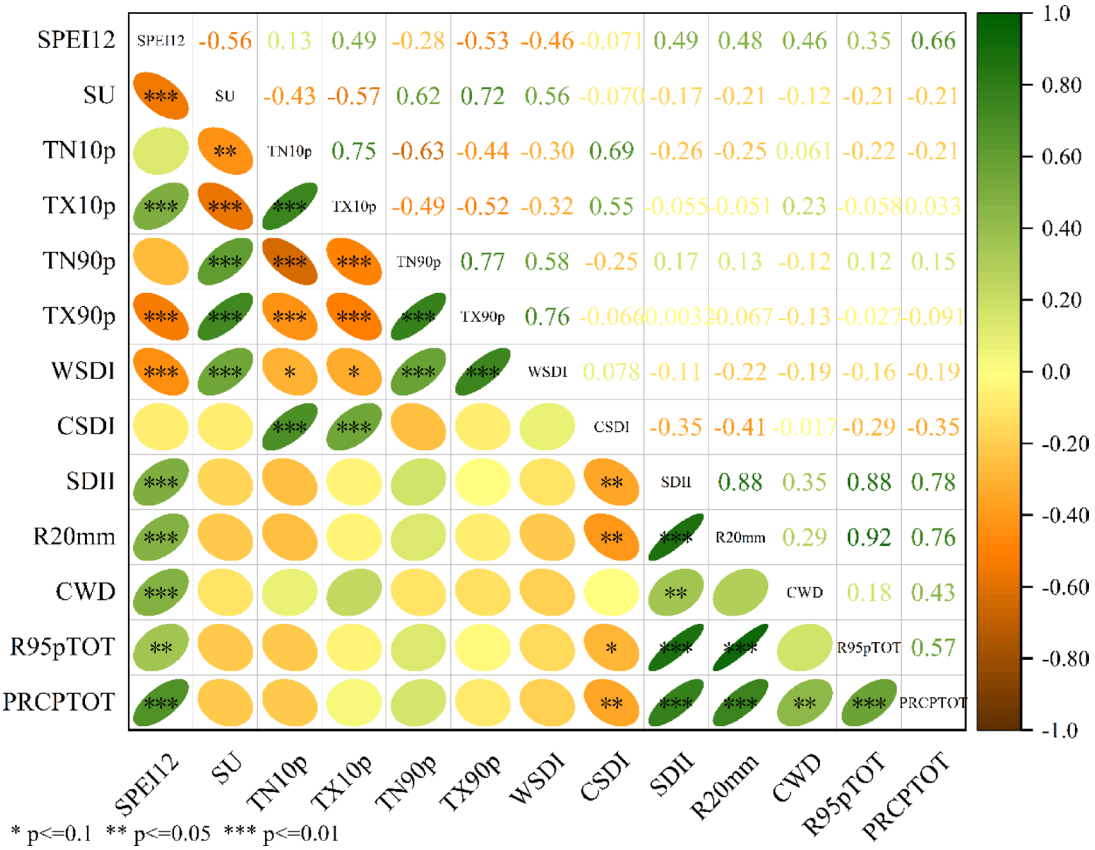

Fig. 10. Pearson correlation Heatmap.

precipitation ≥ 20mm (R20mm), simple daily intensity index (SDII), and cold days (TX10p). Conversely, it was negatively correlated with the summer days (SU), warm days (TX90p), and the warm spell duration index (WSDI).

Among these correlations, SPEI showed a highly significant positive correlation with PRCPTOT and a highly significant negative correlation with SU (both at $^{*}p^{*} \leq 0.01$). Meteorological drought was most strongly influenced by PRCPTOT and SU, while it was least affected by total precipitation on very wet days (R95pTOT) and thecold nights (TN10p). These results suggest that increased annual precipitation corresponds to higher SPEI values—indicating a trend toward wetter conditions—whereas more summer days are associated with lower SPEI, reflecting intensified drought.

Analysis of driving factors based on machine learning

Several nonlinear fitting algorithms—including Decision Tree Regressor, Random Forest Regressor, Support Vector Regressor (with RBF kernel), XGBoost Regressor, Network Regressor, and Gaussian Process Regressor—were employed for model fitting. The coefficient of determination (R^2) was used to quantify the proportion of variance explained by the model[40], hough it does not convey prediction error. In contrast, the root mean square error (RMSE) reflects the accuracy of model predictions[41].

Results (Fig. 11) indicate that XGBoost achieved the best performance, with an R^2 of 0.8335 and an RMSE of 0.265. Based on this, an SPEI12 prediction model was developed using XGBoost. Bayesian optimization was applied to determine the optimal hyperparameters: a maximum tree depth of 3, a learning rate of 0.096, L1 regularization of 0.0187, and L2 regularization of 0.0124. The dataset was split into 80% for training and 20% for testing. Through incremental learning and early stopping, the optimal number of iterations was identified as 62.

The model exhibited excellent performance on both the training set ($R^2 = 0.94$, RMSE = 0.21) and the test set ($R^2 = 0.91$, RMSE = 0.25), indicating strong predictive capability, high generalization capacity, and no signs of overfitting. Overall, the model demonstrates high effectiveness and fulfills the required prediction standards.

To further investigate the driving factors of meteorological drought, SHAP (SHapley Additive exPlanations) analysis was employed. As illustrated in Fig. 12a, annual total precipitation (PRCPTOT) is the primary driver of changes in meteorological drought (SPEI12), with the highest mean absolute SHAP value of 0.245, confirming the dominant role of precipitation. The cold days (TX10p) and the summer days (SU) rank second and third, with mean absolute SHAP values of 0.198 and 0.154, respectively. While Pearson correlation analysis identified PRCPTOT, SU, and the days with precipitation ≥ 20mm (R20mm) as the top three influential factors, SHAP analysis reveals that TX10p and SU may significantly influence drought through nonlinear mechanisms.

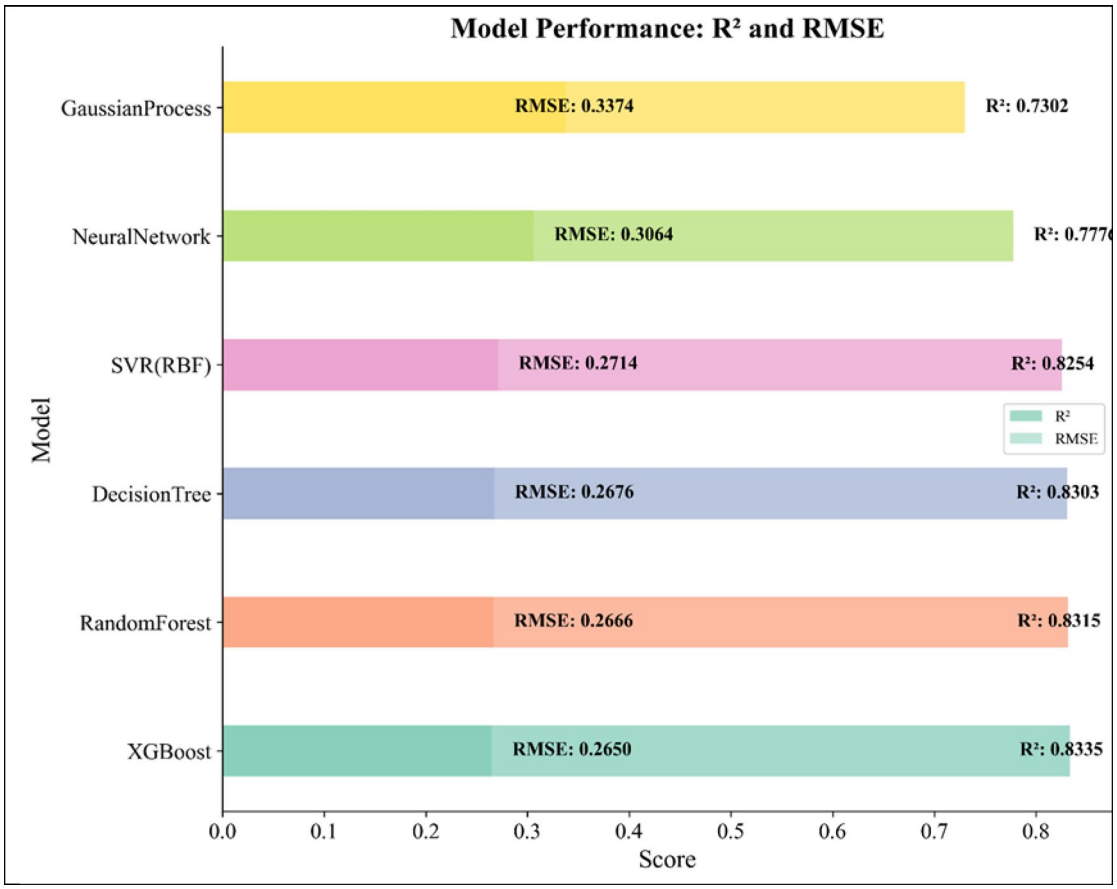

Fig. 11. Model Evaluation.

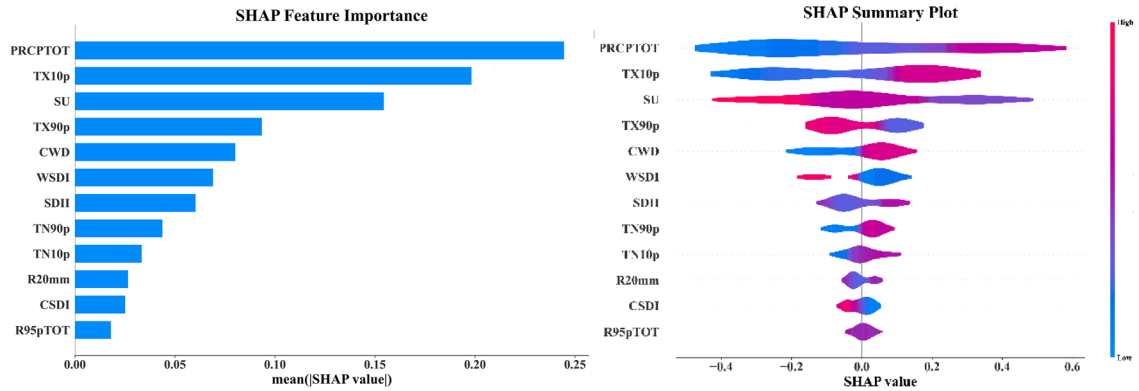

(a) SHAP Importance Evaluation (b) SHAP Summary Plot

Fig. 12. SHAP importance and summary plot.

The SHAP contributions of the warm days (TX90p), consecutive wet days (CWD), and warm spell duration index (WSDI) are 0.093, 0.08, and 0.069, respectively—significantly lower than those of PRCPTOT, TX10p, and SU. By integrating Pearson correlation analysis with SHAP interpretation, this study not only identifies the key drivers of meteorological drought and confirms the importance of annual precipitation, but also uncovers nonlinear relationships that cannot be captured by correlation analysis alone.

To quantify the relative contributions of different variables, the absolute Shapley values were averaged and normalized to sum to 100%. Among the 12 extreme climate indices, PRCPTOT, TX10p, and SU emerge as the top three drivers, contributing 23.35%, 18.93%, and 14.75%, respectively, to the model output. Other variables such as TX90p, CWD, WSDI, and SDII have relatively minor impacts, with contributions of 8.92%, 7.66%,

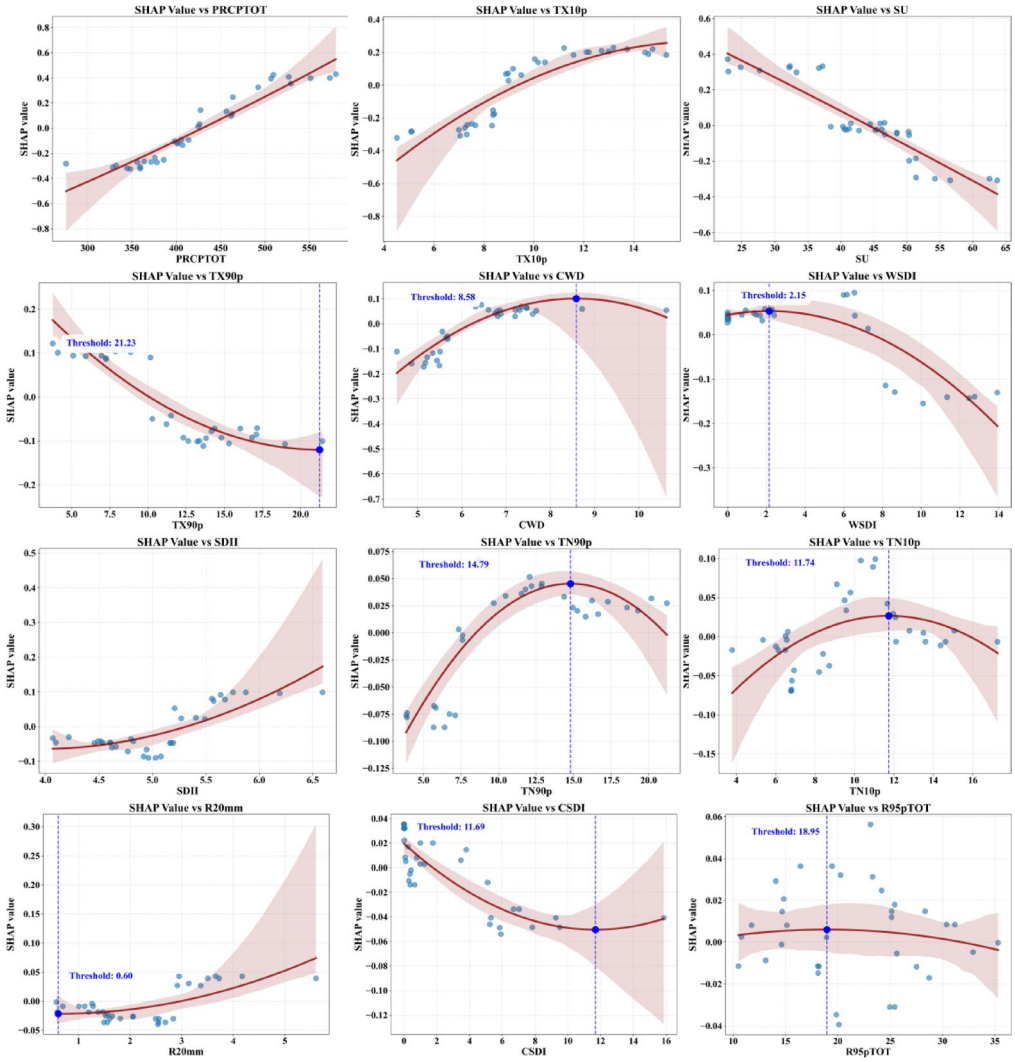

Fig. 13. Diagram of the dependence relationship between extreme factors and meteorological drought.

6.60%, and 5.80%, respectively. The remaining indices—TN90p, TN10p, R20mm, CSDI, and R95pTOT—each contribute less than 5%.

Figure 12b further illustrates the direction of influence of each variable. When an increase in a feature value corresponds to a positive SHAP value, it indicates that the variable contributes to higher SPEI values (reduced drought). PRCPTOT, TX10p, CWD, SDII, TN10p and TN90p exhibit such positive effects, suggesting they alleviate aridification. Conversely, SU, TX90p, WSDI show negative relationships, indicating they intensify drought conditions. Meanwhile, R20mm, CSDI, and R95pTOT are distributed near zero SHAP values, reflecting their minimal contribution to SPEI12 predictions.

To better elucidate the influence of dominant factors on SPEI12, this study employed SHAP (SHapley Additive exPlanations) visualization to rank all factors by importance, thereby intuitively revealing the impact of different extreme climate indices on SPEI12 predictions.

As shown in Fig. 13, PRCPTOT (annual total precipitation) exhibits a clear linear relationship with SHAP values: as precipitation increases, SHAP values consistently rise, indicating a direct humidifying effect on drought conditions. Similarly, TX10p (cold days) also contributes to humidification, though in a nonlinear manner, with the rate of moisture increase slowing as TX10p rises. In contrast, SU (summer days) shows a straightforward negative influence, where more summer days directly intensify aridification.

TX90p (warm days) and CSDI (cold spell duration index) display threshold-based behaviors. For TX90p, values below 21.23% enhance aridification, with the effect diminishing as the threshold is approached. CSDI exhibits a dual pattern: below 11.69%, it promotes aridification, while above this value, it favors humidification.

CWD (consecutive wet days) demonstrates a notable nonlinear relationship. Below 8.58 days, it contributes to humidification at a decelerating rate; beyond this threshold, however, it begins to promote aridification. This may be because short wet spells replenish soil moisture, whereas prolonged precipitation increases runoff or evaporation, reducing water use efficiency.

WSDI (warm spell duration index), TN90p (warm nights), TN10p (cold nights), and R95pTOT (total precipitation on very wet days) all follow similar threshold-dependent patterns, with respective thresholds of 2.15 days, 14.79%, 11.74%, and 18.95%. Notably, R95pTOT has only a minor influence on SHAP values. Meanwhile, both SDII (simple daily intensity index) and R20mm (days with precipitation ≥ 20mm) promote humidification at an accelerating rate as they increase.

Overall, the analysis reveals that most extreme climate indices exhibit complex nonlinear relationships with meteorological drought, often involving specific risk thresholds (as seen with CWD, TX90p, and WSDI). In contrast, SU and PRCPTOT maintain simple linear relationships with SPEI12.

Discussion

Aridification and extreme climate change trends

The persistent aridification trend observed in the water-receiving area of China's Tao River Diversion Project aligns closely with the documented warm-dry pattern across Northwest China[42,43]. This trend is further corroborated by pronounced changes in extreme climate indices: a marked increase in warm extremes (SU, TX90p, TN90p), a decline in cold extremes (TX10p, TN10p), and an overall rise in extreme precipitation indicators (R20mm, R95pTOT, PRCPTOT). These shifts collectively reflect the sharp increases in both temperature and precipitation that Northwest China has experienced over the past half-century[44]. The complexity of precipitation variability in the region may be attributed to Gansu Province's location in central Eurasia, where interactions between the Western Pacific Monsoon and westerly flows from the Mediterranean, Black Sea, and North Atlantic shape local rainfall patterns, resulting in a highly variable and intricate extreme precipitation regime[45].

Explanation of lag response

Wavelet analysis reveals distinct correlation and lag effects between meteorological drought and extreme climate indices. The observed negative correlation and lagged response of drought to extreme high temperatures may be attributed to accumulated heat stress leading to sustained moisture loss, while increased temperatures enhance evapotranspiration from the land surface, thereby delaying drought recovery. This interpretation is consistent with existing studies reporting a gradual rise in evapotranspiration across Northwest China[46]. Conversely, meteorological drought exhibits a leading response and positive correlation with extreme precipitation indices (e.g., SDII and R20mm), suggesting that increased extreme precipitation provides short-term drought alleviation. The short-term resonance period between extreme high temperature and drought contrasts with the longer resonance period observed for extreme precipitation. This indicates that while temperature directly drives drought onset, precipitation plays a moderating role that operates over longer time scales. These findings collectively underscore that temperature remains the dominant factor influencing drought dynamics in the arid inland regions of Northwest China[47].

Discovery of nonlinear threshold effect

The XGBoost-SHAP model effectively quantified the contribution rates and nonlinear thresholds of extreme climate factors influencing drought in the water-receiving area of the Tao River Diversion Project. Among these factors, annual total precipitation (PRCPTOT) is the most important variable alleviating drought, with a contribution rate of 23.35%, followed by the cold days (TX10p) at 18.93%. A notable threshold effect was observed for consecutive wet days (CWD). When CWD exceeds 8.58 days, it may paradoxically intensify drought, likely because prolonged rainfall increases surface runoff and reduces water infiltration efficiency. Similarly, the warm nights (TN90p) and cold nights (TN10p) exhibit threshold behaviors at 14.79% and 11.74%, respectively. In contrast, the cold spell duration index (CSDI) shows an opposite pattern: values below 11.69 days exacerbate drought, while those above this threshold alleviate it. This can be explained by the fact that shorter cold spells (low CSDI) in winter lead to early soil thaw and enhanced evaporation before spring, intensifying aridification. Conversely, longer cold spells promote the formation of stable snow cover, which preserves water for spring and reduces evaporation losses during the non-growing season.

Limitations and prospects

This study has several limitations that point to valuable directions for future research. Although the CHM_Drought dataset was employed to alleviate the limitations posed by sparse meteorological station coverage, uncertainties in data representation may still persist at small spatial scales. Furthermore, the temporal scope of the data is limited to records up to 2018, excluding more recent years that could provide additional insights. In terms of climate indicators, the selection of extreme climate indices did not include weak precipitation measures, which hold relevance for understanding drought mechanisms and should be incorporated in subsequent studies.

Additionally, the use of annual-scale data may obscure important seasonal or sub-seasonal variations in meteorological drought (SPEI) and extreme climate events. Given the strong seasonality typically exhibited by droughts and extreme climate phenomena, future analyses would benefit from adopting a seasonal or monthly analytical framework. While the machine learning models demonstrated strong capability in identifying complex patterns and relationships, their capacity to elucidate the underlying physical mechanisms remains limited. Future work should integrate reanalysis data to explore the synergistic effects of large-scale climate drivers, such as ENSO, on regional extreme climate patterns and drought dynamics.

Recommendations for regional water resources management

The observed warm-drying trend underscores the inadequacy of relying solely on local precipitation to ensure regional water security. In response, the agricultural sector should proactively adjust cropping structures and promote water-saving technologies to mitigate the increasing evapotranspiration pressure driven by persistent warming. Among precipitation-related factors, annual total precipitation (PRCPTOT) is identified as the

primary variable alleviating drought, with a contribution rate of 23.35%. It is thus advisable to leverage water storage infrastructure, such as reservoirs, in years with higher PRCPTOT to build strategic reserves and buffer against uncertainties in interannual precipitation variability. Furthermore, the nonlinear thresholds derived from the machine learning model can serve as critical benchmarks for drought early warning. Study recommend that relevant agencies integrate these key drivers into a comprehensive monitoring and risk-alert framework to enhance drought preparedness and adaptive resource management.

Conclusions

(1) From 1985 to 2018, the SPEI12 index in the water-receiving area of the Tao River Diversion Project revealed a gradual yet persistent aridification trend, marked by a pivotal transition point around 1988. The summer days (SU) increased significantly, as did the warm days and nights. Conversely, a pronounced decline was observed in cold nights and cold days. Although most extreme precipitation indices exhibited mild increases, their overall trends were not statistically significant.
(2) The relationship between meteorological drought (represented by SPEI) and extreme climate indices is complex and nonlinear. SPEI was negatively correlated with extreme temperature indices but positively correlated with extreme precipitation indices. On shorter time scales, most extreme climate indices exhibited significant resonance periods with SPEI, reflecting the rapid influence of changing weather conditions on drought. In contrast, extreme precipitation indices showed resonance over longer time scales.
(3) The main drivers of meteorological drought were identified as annual total precipitation (PRCPTOT, 23.35%), the cold days (TX10p, 18.93%), and the summer days (SU, 14.75%). Increased annual precipitation significantly alleviates drought conditions, while most extreme climate indices exhibit nonlinear relationships with SPEI.

Data availability

The SPEI index was derived from the CHM_Drought dataset (https://zenodo.org/records/14,634,774), a raster dataset with a spatial resolution of 0.1° × 0.1°. This dataset is robust and capable of accurately capturing drought events across mainland China. The SPEI-12 index, covering the period from 1985 to December 2018, was selected for analysis. ArcMap 10.8 was used to crop and mask the downloaded data, enabling the extraction of SPEI data at various scales. Extreme climate data were obtained from the dataset provided by the National Cryosphere Desert Data Center (http://www.ncdc.ac.cn), an NC-format dataset with a spatial resolution of 0.1° × 0.1°.

Received: 23 August 2025; Accepted: 27 October 2025
Published online: 26 November 2025

References

1. Abbas, H. & Ali, Z. A novel statistical framework of drought projection by improving ensemble future climate model simulations under various climate change scenarios. *Environ. Monit. Assess.* **196**, 938 (2024).
2. Jiang, Z. et al. Extreme climate events in China: IPCC-AR4 model evaluation and projection. *Clim. Change* **110**, 385–401 (2012).
3. Zhong, Y. et al. Seasonal drought classification and its characteristics in the red soil region of southern China. *J. Hydrol.: Regional Stud.* **60**, 102587–102587 (2025).
4. Cancelliere, A., Mauro, G. D., Bonaccorso, B. & Rossi, G. Drought forecasting using the standardized precipitation index. *Water Resour. Manage* **21**, 801–819 (2007).
5. Vicente-Serrano, S. M., Beguería, S. & López-Moreno, J. I. A multiscalar drought index sensitive to global warming: The standardized precipitation evapotranspiration index. *J. Clim.* **23**, 1696–1718 (2010).
6. Shukla, S. & Wood, A. W. Use of a standardized runoff index for characterizing hydrologic drought. *Geophys. Res. Lett.* **35**, 2405-2401–2405-2407 (2008).
7. Wells, N., Goddard, S. & Hayes, M. J. A self-calibrating Palmer drought severity index. *J. Clim.* **17**, 2335–2351 (2004).
8. Liu, Q. et al. The optimal applications of scPDSI and SPEI in characterizing meteorological drought, agricultural drought and terrestrial water availability on a global scale. *Sci. Tot. Environ.* **952**, 175933. https://doi.org/10.1016/j.Scitotenv.2024.175933 (2024).
9. Jehanzaib, M., Shah, S. A., Yoo, J. & Kim, T.-W. Investigating the impacts of climate change and human activities on hydrological drought using non-stationary approaches. *J. Hydrol.* **588**, 125052 (2020).
10. Shah, W., Chen, J. & Naseer, S. Climate change and crop yields in Pakistan: A machine learning approach to understanding temperature extremes and drought effects on wheat and rice. *Theoret. Appl. Climatol.* **156**, 536–536. https://doi.org/10.1007/s00704-025-05759-7 (2025).
11. Wilson, A. B., Avila-Diaz, A., Oliveira, L. F., Zuluaga, C. F. & Mark, B. Climate extremes and their impacts on agriculture across the Eastern Corn Belt Region of the U.S. *Weather Climate Extremes* **37**, 100467. https://doi.org/10.1016/j.Wace.2022.100467 (2022).
12. Jamalzi, A. R., Rahman, G., Akhtar, F., Ikram, Q. D. & Kwon, H. H. Spatiotemporal assessment and trend analysis of meteorological drought in Afghanistan (1974–2023) using SPI and SPEI indices. *J. Hydrol.: Regional Stud.* **61**, 102711–102711. https://doi.org/10.1016/j.Ejrh.2025.102711 (2025).
13. Hui, Y. & Fuqing, B. Study on spatiotemporal evolution and driving forces of meteorological drought in the Yellow River Basin considering spatial heterogeneity. *China Rural Water Hydropower* **2**, 74–80 (2025).
14. Qu, Z. C., Huang, S., Liu, S., Wang, L. & Liu, D. Extreme climate and its impact on hydrological drought in the Xilin River Basin of Inner Mongolia over the past 60 years. *Acta Ecol. Sin.* **45**, 5386–5397 (2025).
15. Sifang, F. et al. Climate change impacts on concurrences of hydrological droughts and high temperature extremes in a semi-arid river basin of China. *J. Arid Environ.* https://doi.org/10.1016/j.Jaridenv.2022.104768 (2022).
16. Zhang, Q. et al. A new high-resolution multi-drought-index dataset for mainland China. *Earth Syst. Sci. Data* **17**, 837–853 (2025).
17. Donat, M. G. et al. Updated analyses of temperature and precipitation extreme indices since the beginning of the twentieth century: The HadEX2 dataset. *J. Geophys. Res.: Atmospheres* **118**, 2098–2118 (2013).
18. Sun, W. et al. Seasonal prediction of spring drought over Northeast China. *J. Appl. Meteorol. Climatol.* **64**, 1017–1032 (2025).
19. Angulo, D. P. et al. Multidecadal changes in hydrological droughts across Sub-Saharan Africa. *J. Hydrol.: Regional Stud.* **60**, 102595–102595 (2025).
20. Mann, H. B. Nonparametric tests against trend. *Econometrica J. Econometric Soc.* **13**, 245–259 (1945).

21. Kendall, M. G. Rank Correlation Methods. (1975).
22. Sen, P. K. Estimates of the regression coefficient based on Kendall's tau. *J. Am. Stat. Assoc.* **63**, 1379–1389 (1968).
23. Swagatika, S. S., Ashok, M., Chandranath, C. & Bhabagrahi, S. Climate-changed versus land-use altered streamflow: A relative contribution assessment using three complementary approaches at a decadal time-spell. *J. Hydrol.* https://doi.org/10.1016/j.Jhydrol.2021.126064 (2021).
24. Petchprayoon, P., Blanken, P. D., Ekkawatpanit, C. & Hussein, K. Hydrological impacts of land use/land cover change in a large river basin in central-northern Thailand. *Int. J. Climatol.* **30**, 1917–1930 (2010).
25. Yanlin, L., Yi, H., Yaru, Z. & Liping, J. Spatiotemporal evolutionary analysis of rainfall erosivity during 1901–2017 in Beijing. China. *Environ. Sci. Pollution Res.* **29**, 2510–2522. https://doi.org/10.1007/s11356-021-15639-y (2021).
26. ZHANG, J. *et al.* Analysis of extreme precipitation changes in Lijiang River Basin based on ITA and Mann-Kendall methods. *Journal of Hohai University(Natural Sciences)* **52**, 15–22 (2024).
27. Shah, S. A., Jehanzaib, M., Kim, M. J., Kwak, D. Y. & Kim, T. W. Spatial and temporal variation of annual and categorized precipitation in the Han River Basin, South Korea. *KSCE J. Civ. Eng.* **26**, 1–12. https://doi.org/10.1007/s12205-022-1194-y (2022).
28. Shah, S. A., Jehanzaib, M., Yoo, J., Hong, S. & Kim, T.-W. Investigation of the effects of climate variability, anthropogenic activities, and climate change on streamflow using multi-model ensembles. *Water* **14**, 512 (2022).
29. Ali, S. S., Muhammad, J., Woon, P. K., Sijung, C. & Woong, K. T. Evaluation and decomposition of factors responsible for alteration in streamflow in lower watersheds of the Han river basin using different Budyko-based functions. *KSCE J. Civ. Eng.* **27**, 903–914. https://doi.org/10.1007/s12205-022-0650-z (2022).
30. Civil, D. O. et al. Investigating the impacts of climate change and human activities on hydrological drought using non-stationary approaches. *J. Hydrol.* https://doi.org/10.1016/j.jhydrol.2020.125052 (2020).
31. Zhao, J. et al. Analysis of temporal and spatial trends of hydro-climatic variables in the Wei River Basin. *Environ. Res.* **139**, 55–64. https://doi.org/10.1016/j.envres.2014.12.028 (2015).
32. Douglas, E. M., Vogel, R. M. & Kroll, C. N. Trends in floods and low flows in the United States: Impact of spatial correlation. *J. Hydrol.* **240**, 90–105. https://doi.org/10.1016/s0022-1694(00)00336-x (2000).
33. Swagatika, S. S., Bhushan, K. S., Ashok, M. & Chandranath, C. Sensitive or resilient catchment?: A Budyko-based modeling approach for climate change and anthropogenic stress under historical to CMIP6 future scenarios. *J. Hydrol.* https://doi.org/10.1016/j.Jhydrol.2023.129651 (2023).
34. Alemu, M. M. et al. Spatiotemporal analysis of drought characteristics across multiple timescales in the upper Blue Nile basin, Ethiopia. *Theoretic. Appl. Climatol.* **156**, 435–435 (2025).
35. Wang, M., Chen, Y., Li, J. & Zhao, Y. Spatiotemporal evolution and driving force analysis of drought characteristics in the Yellow River Basin. *Ecol. Ind.* **170**, 113007–113007 (2025).
36. Nourani, V., Tootoonchi, R. & Andaryani, S. Investigation of climate, land cover and lake level pattern changes and interactions using remotely sensed data and wavelet analysis. *Ecol. Inform.* **64**, 101330 (2021).
37. Abdul, F. M. et al. Implications of rainfall variability on groundwater recharge and sustainable management in South Asian capitals: An in-depth analysis using Mann Kendall tests, continuous wavelet coherence, and innovative trend analysis. *Groundwater Sustain. Develop.* **24**, 101060 (2024).
38. Yang, K., Ma, Y. & Tang, Q. Visualisation of key thresholds of crop production potential and their future distribution patterns in china under climate change scenarios. *J. Geovisual. Spatial Analysis* **9**, 33–33 (2025).
39. Zhang, F. et al. Simulation and explanatory analysis of dissolved oxygen dynamics in Lake Ulansuhai, China. *J. Hydrol.: Regional Stud.* **57**, 102109–102109 (2025).
40. Villasante, A., Serrano, Á. F., Sequera, C. O. & Hermoso, E. Methodology for stiffness prediction in structural timber using cross-validation RMSE analysis. *J. Build. Eng.* **107**, 112767–112767. https://doi.org/10.1016/j.Jobe.2025.112767 (2025).
41. Alexander, D. L., Tropsha, A. & Winkler, D. A. Beware of R 2: simple, unambiguous assessment of the prediction accuracy of QSAR and QSPR models. *J. Chem. Inf. Model.* **55**, 1316–1322 (2015).
42. Li, M., Wang, X., Sun, D., Ma, Y. & Feng, X. Analysis of spatiotemporal evolution characteristics of meteorological droughts in Gansu Province based on SPEI. *Res. Soil Water Conserv.* **32**, 191–200 (2025).
43. Chen, S., Men, B., Pang, J., Bian, Z. & Wang, H. Historical and projected extreme climate changes in the upper Yellow River Basin, China. *Sci. Rep.* **15**, 19061–19061 (2025).
44. Chen, Y., Li, Z., Fan, Y., Wang, H. & Deng, H. Progress and prospects of climate change impacts on hydrology in the arid region of northwest China. *Environ. Res.* **139**, 11–19. https://doi.org/10.1016/j.envres.2014.12.029 (2015).
45. An, D. et al. Evidence of climate shift for temperature and precipitation extremes across Gansu Province in China. *Theoret. Appl. Climatol.* **139**, 1137–1149. https://doi.org/10.1007/s00704-019-03041-1 (2020).
46. Haojing, C. et al. Spatial patterns of climate change and associated climate hazards in Northwest China. *Sci. Rep.* **13**, 10418–10418. https://doi.org/10.1038/s41598-023-37349-w (2023).
47. Jin, H. et al. Spatiotemporal evolution of drought status and its driving factors attribution in China. *Sci. Total Environ.* **958**, 178131–178131. https://doi.org/10.1016/j.Scitotenv.2024.178131 (2025).

Author contributions

Conceptualization, H. M. H. and D. M. Z.; Data curation, Z. J. B. and H. H. L.; Formal analysis, J. X. B.; Investigation, J. D. W., Y. F. C. and F. G.; Methodology, H. M. H. and D. L.; Project administration, H. M. H., D. M. Z; Software, D. L. and C. J. C.; Supervision, J. D. W.; Validation, J. X. B., C. J. C., F. G. and H. H. L.; Visualization, D. L.; Writing—original draft, H. M. H and D. L; Writing—review and editing, D. L., D. M. Z., C. J. C. and H. H. L. All authors have read and agreed to the published version of the manuscript.

Funding

This study was supported by the Gansu provincial key research and development program (23YFFA0018); Gansu Province Water Conservancy Research and Planning Project(23GSLK044).

Declarations

Competing interests

The authors declare no competing interests.

Ethics approval

There are no ethical issues in choosing the Water-Receiving Area of the Tao River Diversion Project as the study region.

Additional information

Correspondence and requests for materials should be addressed to D.L.

Reprints and permissions information is available at www.nature.com/reprints.

Publisher's note Springer Nature remains neutral with regard to jurisdictional claims in published maps and institutional affiliations.